Supplemental Information for

Permeation of CO_2 and N_2 Through Glassy Poly(Dimethyl Phenylene) Oxide (PPO) under Steady and Pre-Steady State Conditions

Marielle Soniat [a,b], Meron Tesfaye [c,d], Amirhossein Mafi[e], Daniel Brooks [e], Nicholas D. Humphrey [e], Lien-Chun Weng [a,d], Boris Merinov [e], William A. Goddard, III [e], Adam Z. Weber [a,c], and Frances A. Houle [,a,b]*

a Joint Center for Artificial Photosynthesis, Lawrence Berkeley National Laboratory, Berkeley, CA 94720, USA

b Chemical Sciences Division, Lawrence Berkeley National Laboratory, Berkeley, CA 94720, USA

c Energy Storage and Distributed Resources Division, Lawrence Berkeley National Laboratory, Berkeley, CA 94720, USA

d Department of Chemical and Biomolecular Engineering, University of California, Berkeley, CA 94720, USA

e Materials and Process Simulation Center (MSC), Beckman Institute, California Institute of Technology, Pasadena, CA 91125, USA

Table of Contents

1. Literature Data on Permeability and Solubility in PPO

Previously published data on permeability and solubility of N_2 and CO_2 are shown for comparison in Figure S5.[1-5] The permeability has greater variation than the solubility. While the variation in the sorbed concentration versus pressure is small, especially at low pressures, the solubility parameters determined using the dual mode model reported in the literature studies, listed in Table S1, can vary greatly. This indicates that the dual mode solubility parameters are non-unique solutions. This conclusion is supported by re-fitting Toi et al.'s data using solubility parameters from the studies of Maeda and Paul[5] and Chern et al.[3] with little loss of accuracy. Table S1 shows these dual mode solubility parameters from the literature, and Figure S2 shows the solubility isotherms using those parameters. A large variation in the parameters can produce a fit within a 10% difference from the data reported by Toi et al. Bondar et al.[6] have previously reported that the best-fit values of the dual mode parameters depend on the pressure range over which the isotherms are investigated.

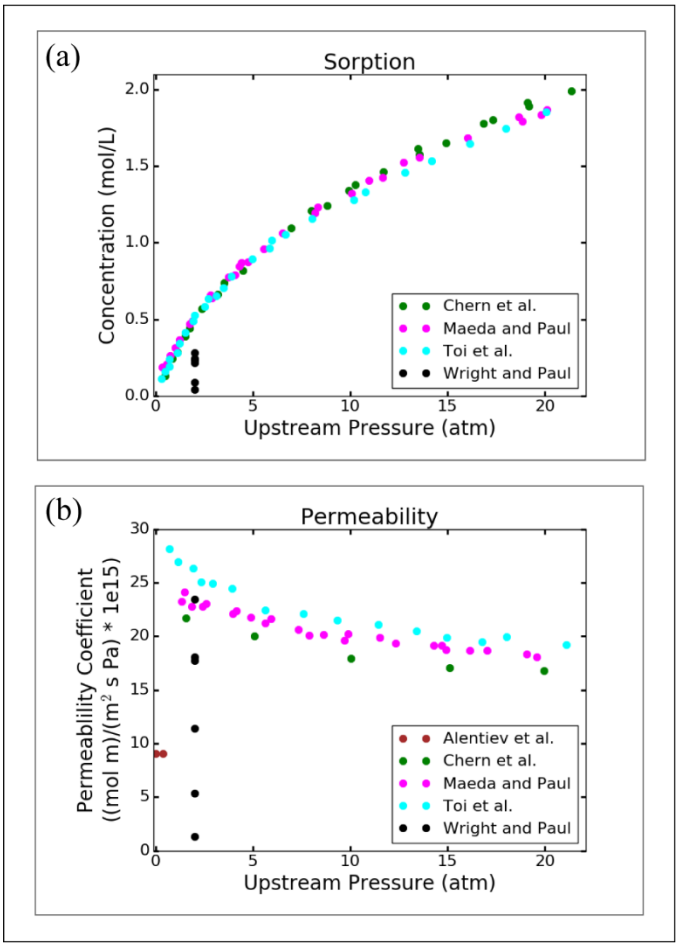

Figure S1. Comparison of from a variety of literature studies on (a) sorption and (b) permeability of CO_2 as a function of upstream pressure.

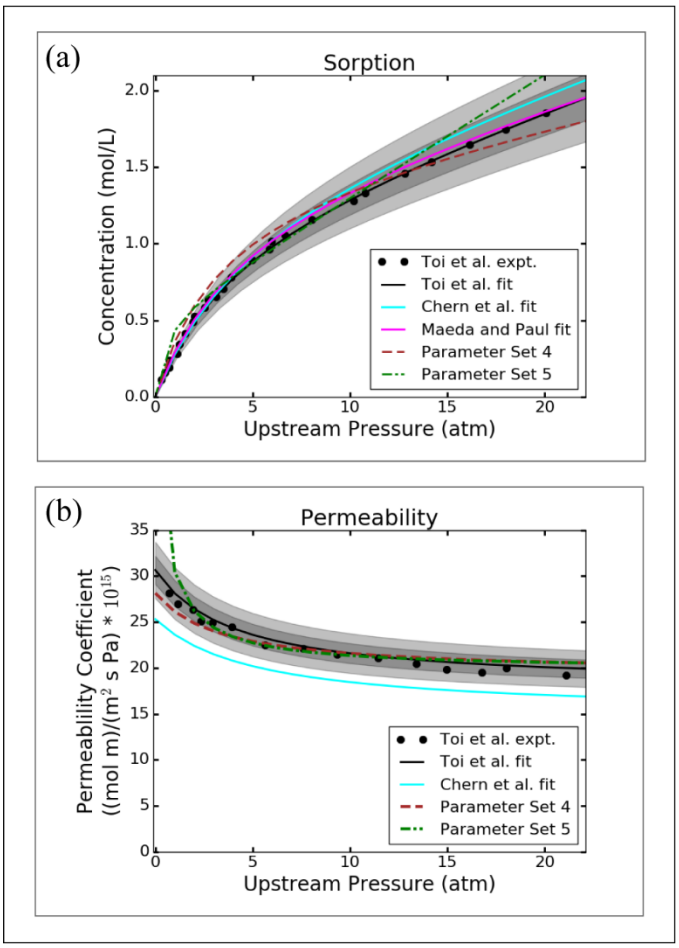

Figure S2. Comparison of (a) sorption and (b) permeability isotherms using varying dual mode parameters listed in Table S XX. The light gray region represents a 5% difference from the data reported by Toi et al, and the dark gray region represents a 10% difference.

Table S1. Dual mode parameters used in Figure S2.

Parameter Set	S_d	S_L	b_L	D_d	D_L	Ref.
	cc(STP)/(cc atm)	cc(STP)/cc	1/atm	cm^2/s	cm^2/s	
1	0.95	27.5	0.25	4.29×10^{-7}	4.18×10^{-8}	[1]
2	0.921	32.74	0.195	3.68×10^{-7}	3.68×10^{-8}	[3]
3	0.788	32.6	0.216			[5]
4	0.55	33	0.3	8×10^{-7}	2×10^{-8}	[a]
5	1.7	12	2	2.5×10^{-7}	2×10^{-8}	[a]

[a] This work.

2. Molecular Metadynamics Methods

We used force field parameters that describe CO_2 as a rigid five-site molecule, where the partial charges and Lennard-jones parameters of O and C were taken from Trappe force field[1]. To describe the momentum inertia accurately, two virtual sites were also defined that carry the ½ of CO_2 mass. By this definition, O and C just have charge and Lennard-jones parameters but no masses. N_2 was also described as a rigid three-site molecule.[7]

The slab of PPO was placed in the middle of the box such two vacuum spaces existed on either side of the PPO (below in Figure S8a & S9a). We inserted 5 gas molecules randomly in one of the vacuum spaces, which levels the pressure of gas phase ~2 atm. We performed a 4 ns of classical molecular simulations with a 1.0 fs time step in the canonical ensemble (NVT) so that the system temperature reached 300 K with some relaxation of the polymer structure. During this calculation, we placed harmonic restraints on the gas molecules with force constants of 1000 kJ/(mol nm^2) to fix their positions and not allow them to penetrate to the polymer. Following the initial structural relaxation, we carried out long free energy calculations for N_2 and CO_2 diffusion across the PPO using well-tempered metadynamics.[8]

3. Additional Details of the Multiscale Model Implementation

The rate for diffusion is calculated by

$$r = -D\,\nabla[X]\,A \qquad \text{(S1)}$$

where r is the forward rate, and $\nabla[X]$ is the gradient in the concentration of X with the distance calculated from the centers of adjacent compartments. The units are converted to particles per second for calculations in the Kinetiscope engine. Diffusion between compartments involves movement from occupied sites in the source compartment to empty sites in the target compartment. The sites are associated with the state of the gas-exposed polymer, Ψ, as described in the main text.

Several interactions are assumed to be diffusion-controlled, for which the rate coefficient is calculated from the Smoluchowski equation,

$$k_{Smoluchowski} = \alpha(\,4\,\pi\,N_{Av}\,D_{AB}\,R_{AB}) \qquad \text{(S2)}$$

where α is the reaction efficiency, N_{Av} is Avogadro's number, D_{AB} is the mutual diffusion coefficient between species A and B, and R_{AB} is the interaction distance between species A and B. In all cases, the reaction efficiency α is assumed to be unity. In general, the Smoluchowski equation should be considered an order of magnitude estimate, and so the simulations were tested for their sensitivity to the values of the rate coefficients calculated using this equation.

The rate coefficient for the change polymer state affecting the gas diffusion coefficient ($k_{D(c)}$ for Reaction 3A) is calculated using $D(p_{up}(CO_2) \sim 10\ atm) = 1.949 \times 10^{-11}\ m^2/s$ from the middle of the pressure range. The van der Waals radii of CO_2 and 1,3 dimethyl benzene[9-10] are

added to get the interaction distance R_{AB}. This gives $k_{D(c)} = 8 \times 10^6$ M^{-1} s^{-1}. The simulations were shown to be insensitive to the precise value of $k_{D(c)}$, presented below.

In the dual mode model, gas adsorption and desorption follow the form in Scheme 1. Transport within the polymer does not occur through independent dissolved and Langmuir diffusion paths. Instead, the diffusion paths are coupled through continuous, diffusion-controlled interchange of solutes, shown in Scheme 4. The diffusion coefficient of CO_2 at low pressure (p_{up} = 1.31 atm) of 9.650×10^{-12} m^2/s is used. The interaction distance is the sum of van der Waals radii of CO_2 (r_{vdW} = 0.20 nm)[11] and benzene (r_{vdW} = 0.27 nm).[12] This results in $k_{exchange} = 2 \times 10^7$ M^{-1} s^{-1}; however, using this value produces an inefficient simulation where most of the computation time was being spent shuffling molecules between dissolved and Langmuir sites. Therefore, for computational efficiency, we allow $k_{exchange} = 10^2$ M^{-1} s^{-1}. The sensitivity to this value was tested, and the results of the sensitivity tests are presented in Section 6 below.

The thicknesses of the compartments used for the gas collection increase exponentially, starting from the one closest to the interface having at thickness of 1 nm, the same thickness as the interface compartment. The final compartments of the gas collector have thicknesses of 0.382366 m for Sample 1, 0.842453 m for Sample 2, and 0.730491 m for Samples 3 and 4; the differences are due to the differing cross-sectional areas of the collection volume, which is held constant at 41.73 cm^3.

4. Correction of Sorption and Permeation Data for Swelling.

Gotthardt et al.[13] report the partial molar volume of CO_2 in a glassy polymer increases from 10 cm^3/mol at low concentration and approaches 46 cm^3/mol (the same as CO_2 in organic solvents) at high concentration.[13] These partial molar volumes correspond to molar densities, ρ, of 100 mol/L and 21.7 mol/L, respectively. The limits of swelling induced in PPO by CO_2 at these molar densities are reported in Figures S3 and S4. At ρ(gas) = 21.7 mol/L, CO_2 will cause a volume dilation >1.2% during sorption, whereas N_2 causes a volume dilation of <1.2% at the pressures used in this study. Visser and Wessling report a dilation threshold of ≥1.2% in a polyimide (Matrimid) for which a volume increase greater than the threshold results in transport behavior that is controlled by a combination of Fickian diffusion and membrane swelling.[14] The dilation threshold for PPO is unknown, but pre-steady state behavior seems to be unaffected by swelling in our samples (see Fig. 6 of the main text).

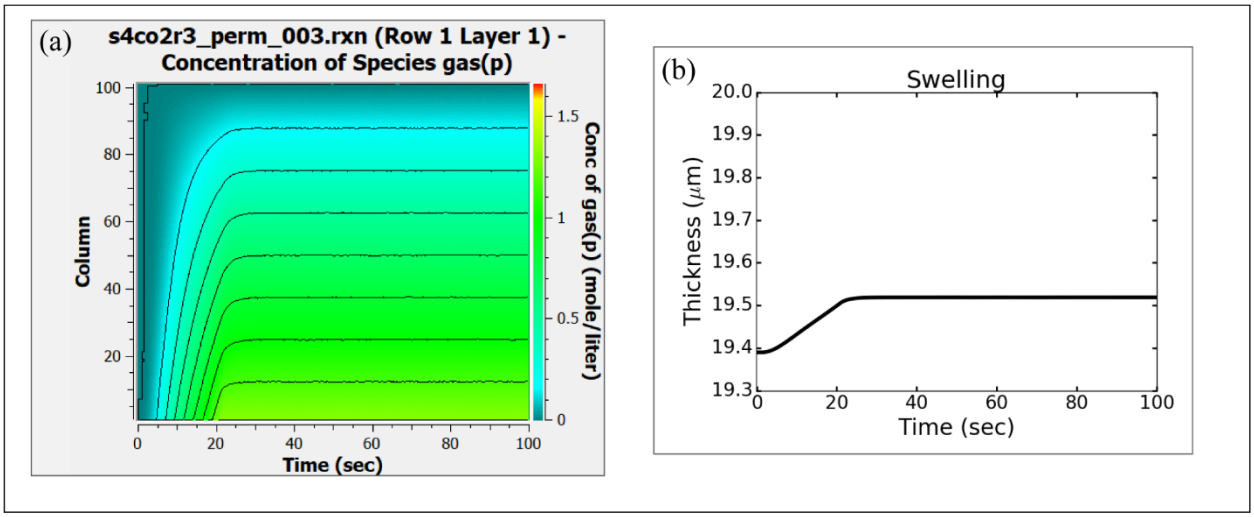

Figure S3. The (a) degree of swelling within the membrane and (b) total thickness change for CO_2 using a molar density of 100 mol/L. The contour plots show the volume of each membrane compartment through the thickness of the membrane on the y-axis over the full time of the simulation on the x-axis. The term "Column" corresponds to the compartment number within the simulation, where the smaller numbers are closest to the upstream interface and the larger numbers are closest to the downstream interface.

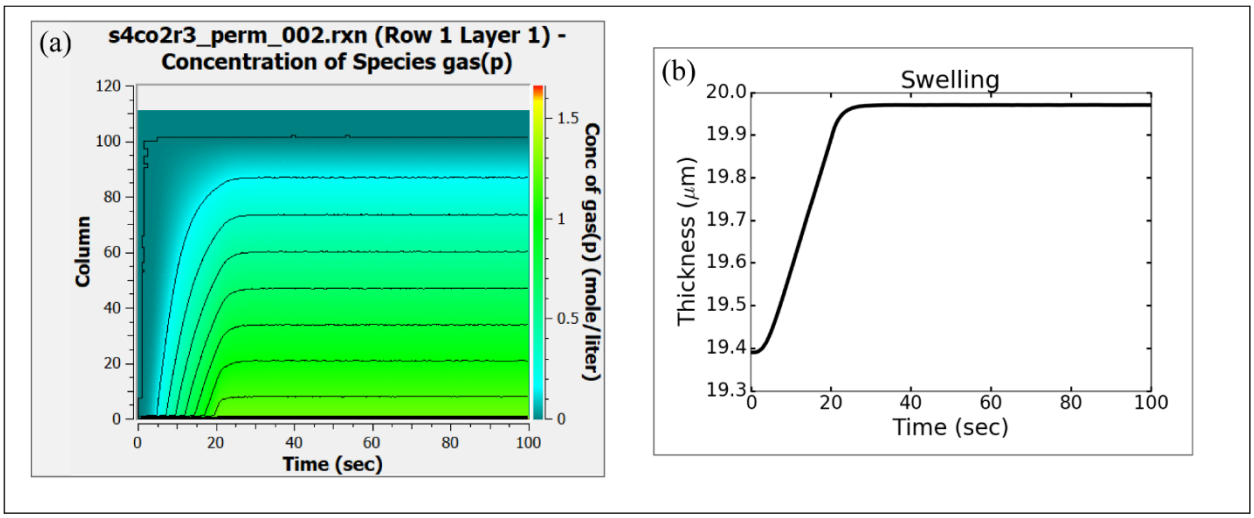

Figure S4. The (a) degree of swelling within the membrane and (b) total thickness change for CO_2 using a molar density of 21.7 mol/L. The contour plots show the volume of each membrane compartment through the thickness of the membrane on the y-axis over the full time of the simulation on the x-axis. The term "Column" corresponds to the compartment number within the simulation, where the smaller numbers are closest to the upstream interface and the larger numbers are closest to the downstream interface.

In the permeation simulation, the gas concentration within the membrane (Figs. S3 and S4) falls linearly from its maximum concentration at the upstream interface to a negligible

concentration at the downstream interface. This results in the membrane swelling near the upstream interface consistent with the degree of swelling in the sorption experiment but no swelling near the downstream interface. Thus, the final membrane thickness increases by about half of the thickness increase during sorption. The experimentally reported permeation data does not take into account the change in thickness. Correcting for swelling results in values of permeability coefficients that increase by <5%.

Finally, the time-dependent permeation for simulations using constant volume, minimum swelling, and maximum swelling is similar, as shown in Figure S5. They all match experiment well if a non-instantaneous equilibration to the upstream pressure rise is used. The slope for the simulation with minimum swelling is slightly too large since D and S were calculated based on the maximum swelling; the D and S for the constant volume simulation were calculated separately.

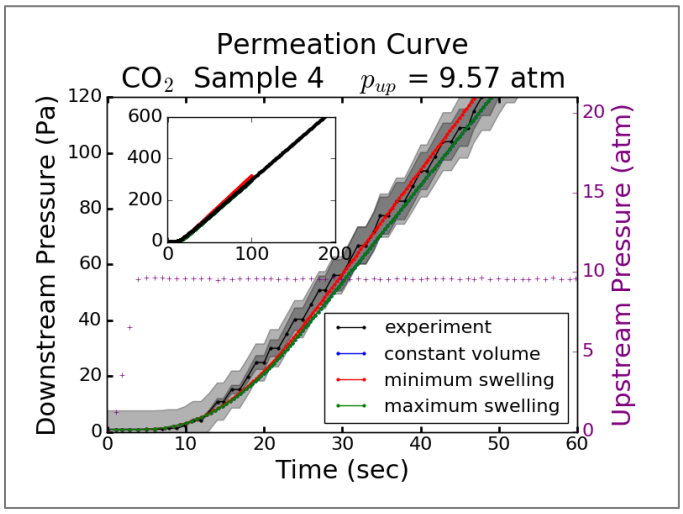

Figure S5. Comparison of time-dependent permeation for simulations using constant volume, minimum swelling, and maximum swelling with a non-instantaneous equilibration to the upstream pressure rise. The curve for maximum swelling lies directly on top of the curve for constant volume.

5. Sensitivity to $k_{D(c)}$

For the results presented in the main text, a diffusion-controlled $k_{D(c)} = 8 \times 10^6$ M^{-1} s^{-1} is used. However, the interaction between gas and polymer may have a slower, reaction-controlled $k_{D(c)}$ for the conversion of the polymer from state Ψ_p to state Ψ_F. Therefore, several additional values of $k_{D(c)}$ are tested for their effect on the simulations of downstream pressure versus time, with results reported in Figure S6. The values tested are arbitrary numbers but span several orders of magnitude. A rate coefficient of 1×10^4 M^{-1} s^{-1} gives exactly the same results as the diffusion-controlled $k_{D(c)}$. A rate coefficient of 1.0 gives very similar results - the increase in downstream pressure starts at the same time, and the steady-state slope is the same, but the non-steady state

behavior is extended over a longer period of time. Once the rate coefficient drops to 0.1, the simulation can nearly capture the time-dependent pre-steady state downstream pressure, but the slope is too low at later times. This is because the simulated system has not yet come to steady-state, whereas the experiment already is at steady state. This comparison of values for $k_{D(c)}$ shows that a slower, reaction-controlled conversion between initial and final diffusion coefficients cannot capture the proper experimental behavior.

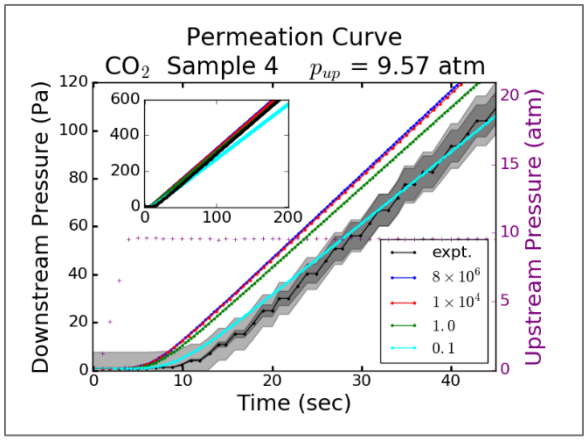

Figure S6. Sensitivity of simulation results to $k_{D(c)}$ for concentration-dependent diffusion coefficients.

6. Sensitivity to $k_{exchange}$

In the main text, simulations are performed using a reduced value of $k_{exchange}$ = 100 M^{-1} s^{-1} instead of its calculated value of 2 × 10^7 M^{-1} s^{-1} for computational efficiency. Figure S7 shows that the simulation results are insensitive to the value of $k_{exchange}$.

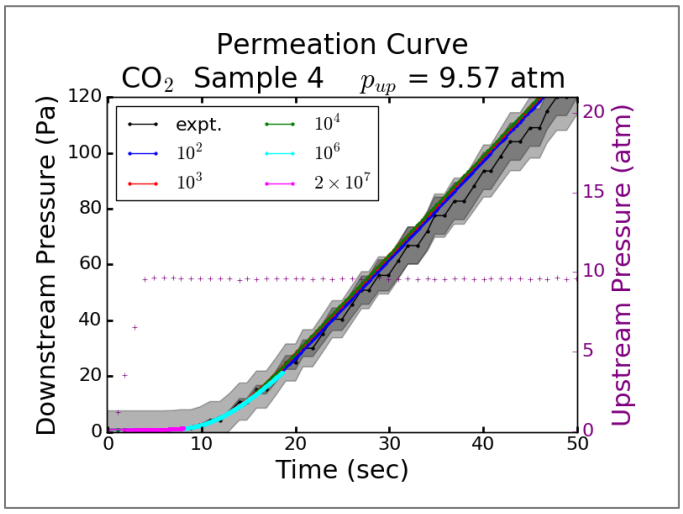

Figure S7. Sensitivity of simulation results to $k_{exchange}$ for the dual mode model.

7. Permeation Experiment Results

The experimental time-dependent downstream pressure curves are shown in Figures S8 and S9 for N_2 and CO_2, respectively.

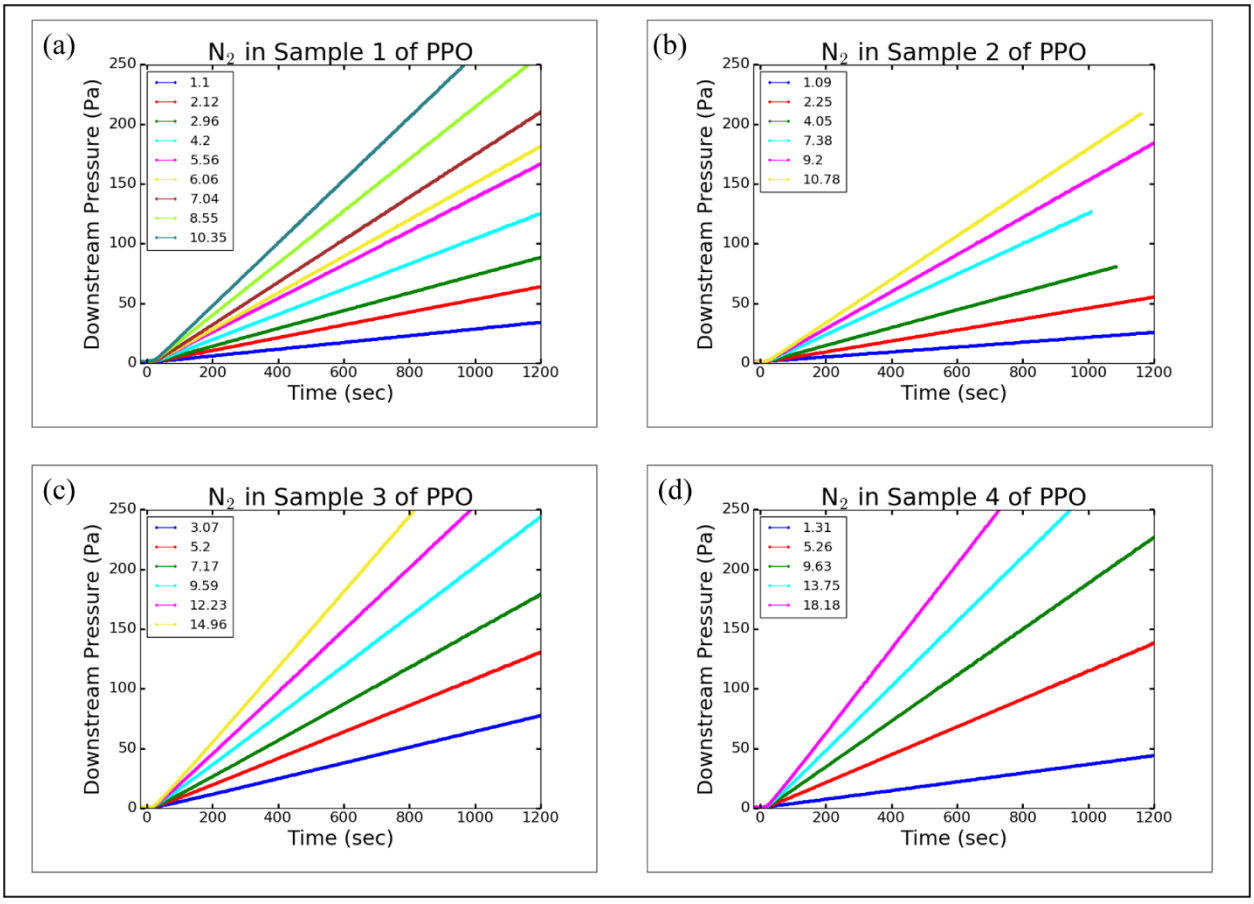

Figure S8. Downstream pressure increase over time for N_2 permeation of PPO through (a) Sample 1, (b) Sample 2, (c) Sample 3, and (d) Sample 4. The legend lists the upstream pressure for each data set.

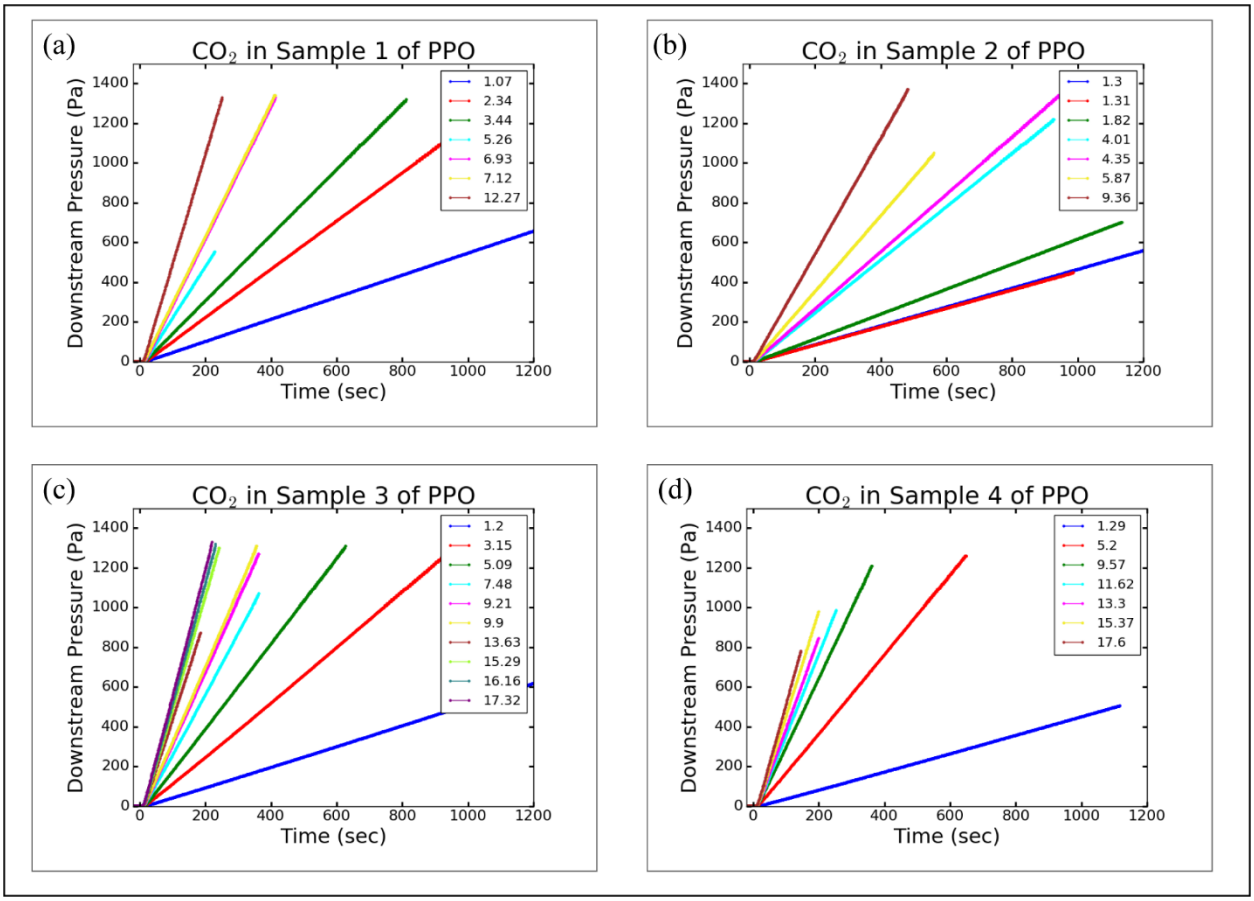

Figure S9. Downstream pressure increase over time for CO_2 permeation of PPO through (a) Sample 1, (b) Sample 2, (c) Sample 3, and (d) Sample 4. The legend lists the upstream pressure for each data set.

8. Correlation of Permeability with Tg and Density

Wright and Paul studied permeability of PPO based on processing conditions.[2] By varying the time and intensity of irradiation during photopolymerization, they produced PPO samples of varying Tg and density. Figure S10 shows the permeability of these samples as a function of Tg (Fig. S10a) and density (Fig S10b) for several gas molecules. The relationship of permeability to Tg is non-monotonic. The permeability increases as density decreases for all the gases studied. This study indicates that the samples in this work should have a higher permeability because they have a lower density than PPO used in most studies in the literature. The correlation between permeability and density may in turn be related to the correlation between permeability and crystallinity[15] in that higher crystallinity produces both higher density and lower permeability. Further comparisons to the literature are inconclusive due to variations in sample processing procedures and inconsistent reporting on density and other material characteristics.

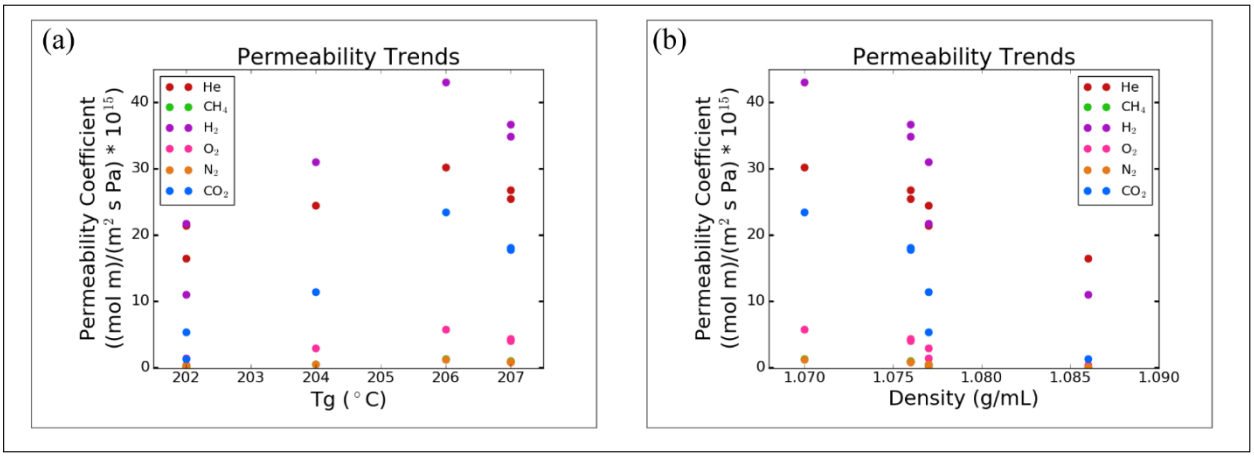

Figure S10. Correlation of permeability to (a) Tg and (b) density using data from Reference [2]. Note that the data points for N_2 lie on top of the data points for CH_4.

9. Linear Fit of Permeability Isotherm

The permeability versus upstream pressure data can be fit with a linear function, $P = m\,p_{up} + b$, where m is the slope and b is the y-intercept, as shown in Figure S11. In this case, b corresponds to the permeability a zero pressure, and $m = S(p)D(p)$. The standard deviation is similar to the dual mode model fit, indicating that the more complex dual mode function may not be necessary.

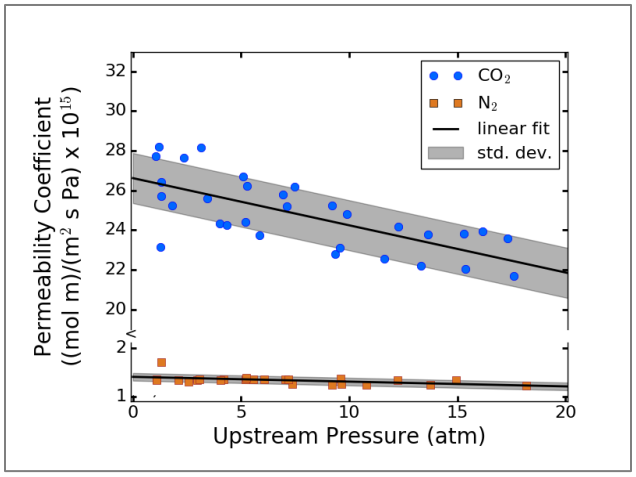

Figure S11. Permeability coefficient as a function of upstream gas pressure for N_2 (orange squares) and CO_2 (blue circles) for all PPO samples. The black lines show a linear fit where $P(N_2) = \left(-0.00980\,p_{up} + 1.40\right) \times 10^{15}$ (mol m)/(m^2 s Pa) with 5.6% standard deviation and $P(CO_2) = \left(-0.238\,p_{up} + 26.6\right) \times 10^{15}$ (mol m)/(m^2 s Pa) with 4.7% standard deviation. The gray area shows one standard deviation from the dual mode fit.

10. Results of Metadynamics Molecular Dynamics Simulations

The metadynamics MD simulations allow for better sampling of the gases' free energy and diffusion within the polymer.[8] The results from the metadynamics MD simulations are shown in Figures S12 for N_2 and S13 for CO_2. Figures S12a and S13a show the PPO polymer slab in light blue with N_2 in dark blue in S12a and CO_2 in red in S13a; the molecules can be seen both in the gas phase and within the polymer. Figure S12b shows the z-position, L_z, of the *biased* N_2 molecule throughout the course of the simulation. Here, the z-direction is normal to the surface of the polymer, as indicated in Figure S12a. Figures S12c - S11f show the z-position of the *unbiased* N_2 molecules throughout the course of the simulations. The biased N_2 molecule crosses the center of the slab (0 position on the y-axis) 4 times in a single simulation, whereas the unbiased N_2 molecules cross the center only once in four separate simulations. Therefore, it is clear that the biased molecule explores a greater region of the PPO structure than an unbiased molecule.

Figure S13b shows the z-position, L_z, of the *biased* CO_2 molecule throughout the course of the simulation, in which CO_2 crosses the center of the slab 6 times. Figures S13c - S13f show the z-position of the *unbiased* CO_2 molecules, which cross the center 20 times in the set of four simulations. Again, it is clear that the biased molecule explores a greater region of the PPO structure than its unbiased counterparts. In addition, the CO_2 molecules move through the full polymer thickness more frequently than N_2.

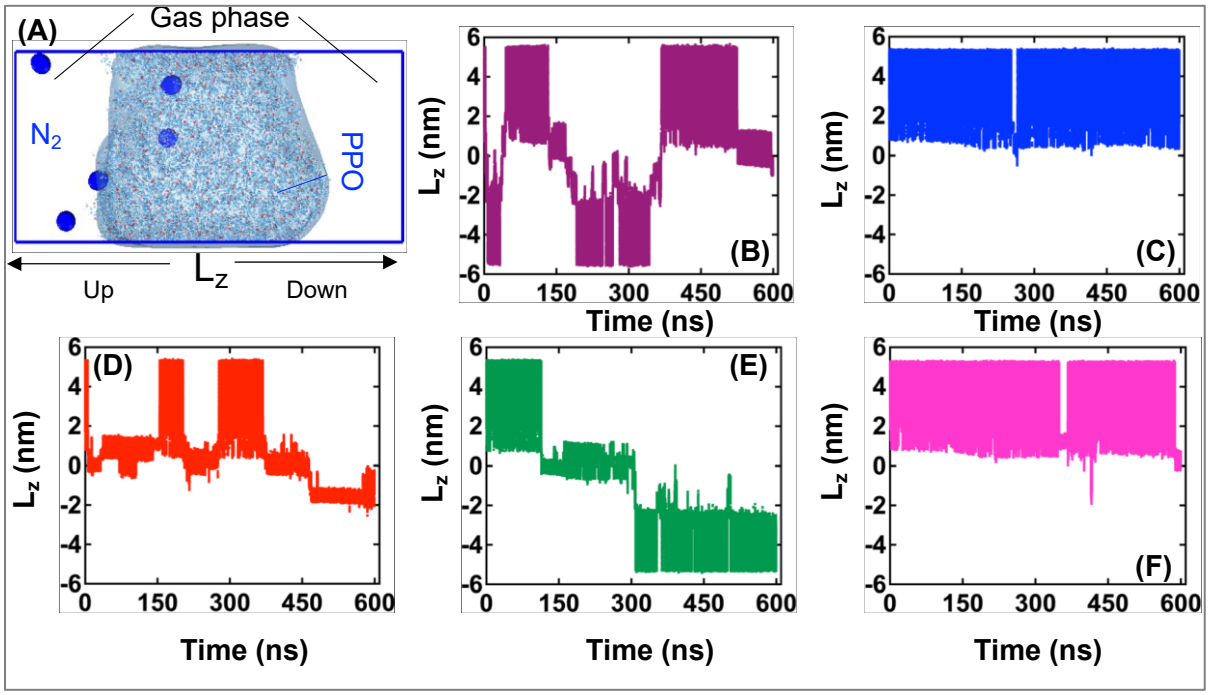

Figure S12. (A) Simulation box including 5 N_2 molecules and 10 chains of PPO polymer. The initial pressure in the gas phase is 2 atm on the upstream side (labeled Up). N_2 are shown with the blue van der Waals spheres. PPO polymer slab is shown a continuum surface. (B) Position in the z-direction, L_z, of the biased N_2 molecule with respect to time. (C), (D), (E), and (F) Position in the z-direction of the un-biased N_2 molecules with respect to time.

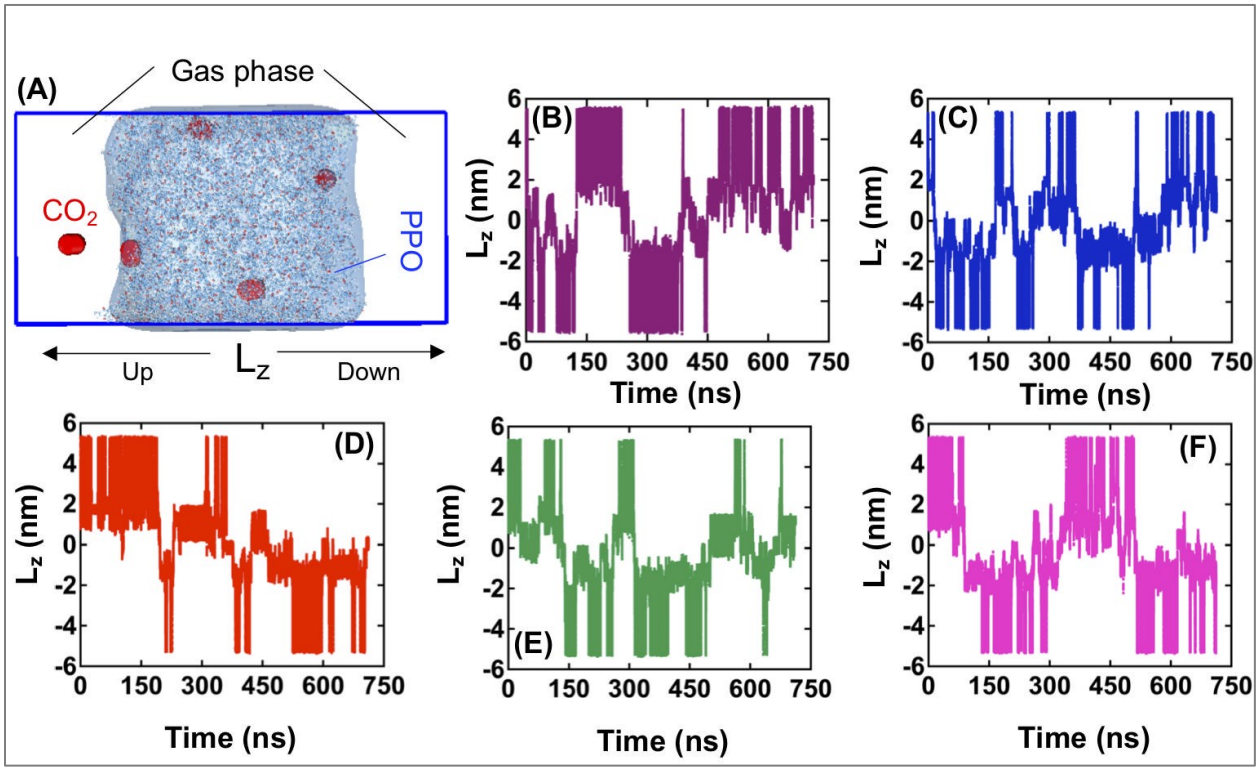

Figure S13. (A) Simulation box including 5 CO_2 molecules and 10 chains of PPO polymer. The initial pressure in the gas phase is 2 atm on the upstream side (labeled Up). CO_2 are shown with the blue van der Waals spheres. PPO polymer slab is shown a continuum surface. (B) Position in the z-direction, L_z, of the biased CO_2 molecule with respect to time. (C), (D), (E), and (F) Position in the z-direction of the un-biased CO_2 molecules with respect to time.

11. Additional Results for Single Mode Model with Delayed Polymer Response

Figures S14 - S16 show additional examples of the agreement between experimental downstream pressure rise and simulations using a single permeation mode for N_2 and CO_2 with a non-instantaneous equilibration of bulk polymer to upstream pressure rise. The different samples are from the same experimental batch, and so the small differences between them result in small quantitative differences but nothing qualitative. Table S2 lists the values for the input variables.

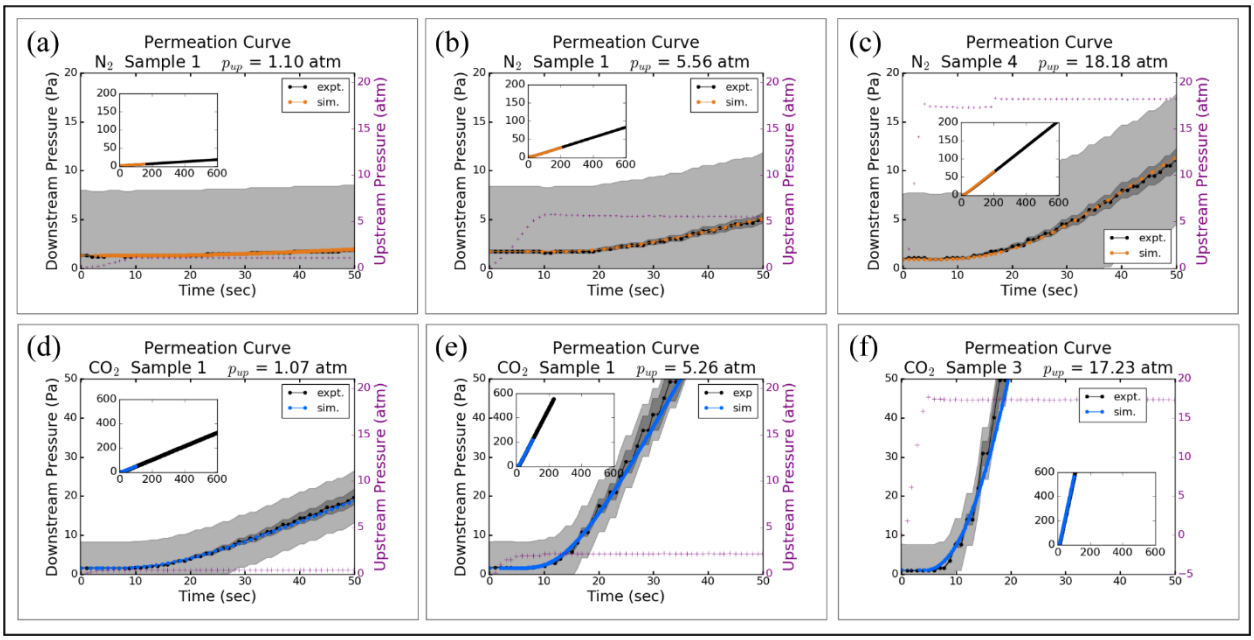

Figure S14. Comparison of simulation and experimental permeation curves for (a-c) N_2 (orange) and (d-f) CO_2 (blue) for the single mode model. The sample number and upstream pressure are shown in the titles. The shaded regions represent the measurement error. The main figures show the downstream pressure rise (black) and upstream pressure rise (purple) over time for the pre-steady state region, and the inset figures show the steady-state region.

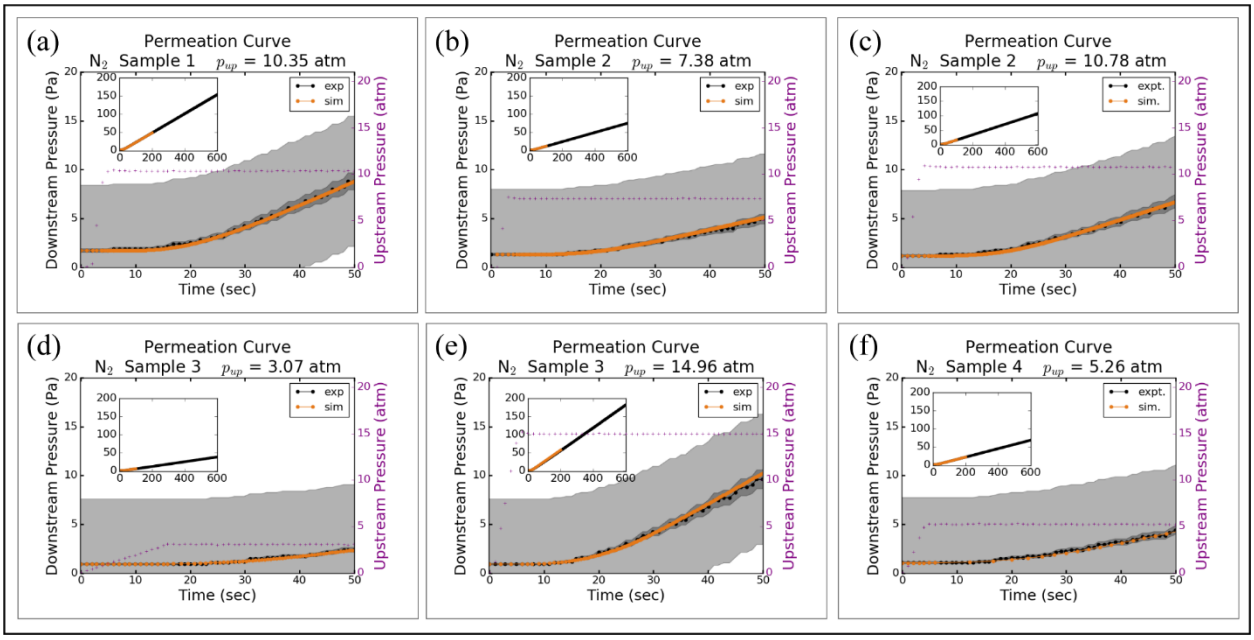

Figure S15. The downstream pressure increase over time as N_2 permeates through PPO using the single mode model. The sample number and upstream pressure are given in the title. The inset

shows the full experimental timescale, and the main figure zooms in on the pre-steady state region. The upstream pressure is included on the right y-axis. The shaded regions represent sample-to-sample deviation of 9%.

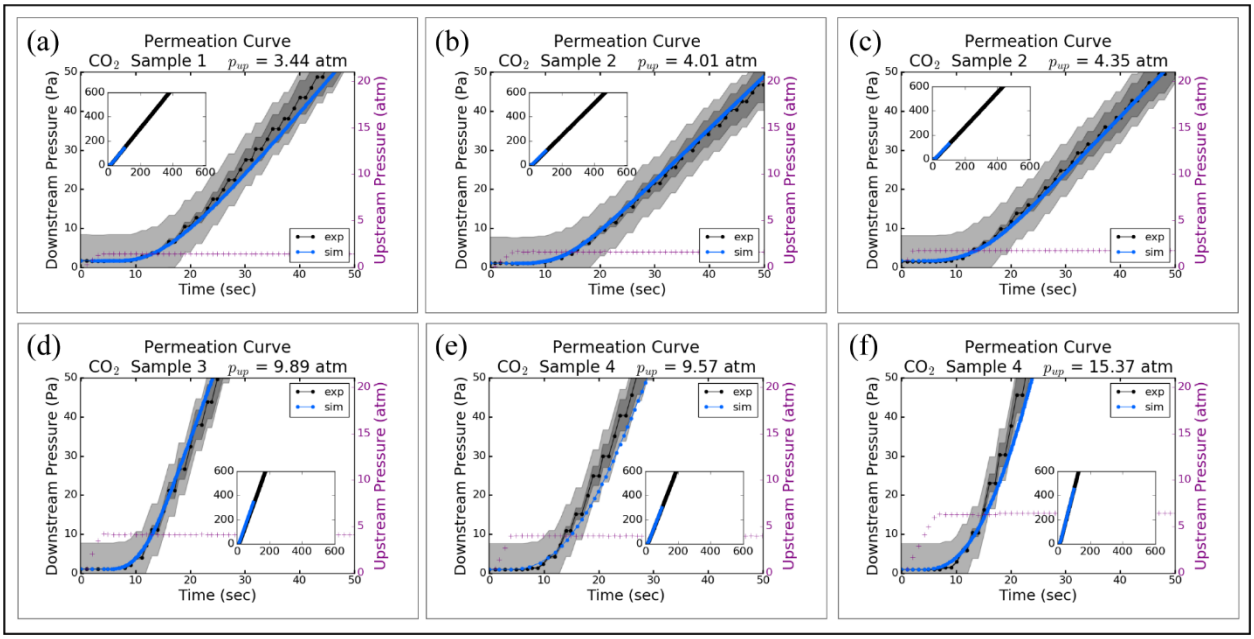

Figure S16. The downstream pressure increase over time as CO_2 permeates through PPO using the single mode model. The sample number and upstream pressure are given in the title. The inset shows the full experimental timescale, and the main figure zooms in on the pre-steady state region. The upstream pressure is included on the right y-axis. The shaded regions represent sample-to-sample deviation of 8%.

Table S2. List of all input variables for the single mode simulations.

Gas	Sample	p_{up}	$[gas(g)]_{init}$	potential [gas(p)] in Ψ_v	maximum [gas(p)] in Ψ_p	k_{rise}	D_{app}
		atm	nmol/L	mol/L	mol/L	M s^{-1}	m^2/s
CO_2	1	1.07	624	0.303	0.299	0.20	1.011×10^{-11}
	1	3.44	676	0.728	0.7043	0.25	1.285×10^{-11}
	1	5.26	624	0.947	0.907	0.22	1.539×10^{-11}
	1	2.34	676	0.559	0.545	0.25	1.212×10^{-11}
	2	4.01	416	0.803	0.774	0.075	1.293×10^{-11}
	2	4.35	572	0.845	0.813	0.060	1.330×10^{-11}
	3	17.32	416	1.854	1.708	0.13	2.461×10^{-11}
	3	9.89	416	1.356	1.276	0.15	1.967×10^{-11}
	4	9.57	364	1.331	1.254	0.070	1.818×10^{-11}
	4	13.30	364	1.597	1.487	0.34	1.995×10^{-11}
	4	15.37	364	1.732	1.604	0.10	2.158×10^{-11}
N_2	1	1.10	520	0.0190	0.0190	0.006	7.911×10^{-12}
	1	5.56	676	0.0865	0.0862	0.015	8.826×10^{-12}
	1	10.35	676	0.147	0.146	0.030	9.704×10^{-12}
	2	7.38	520	0.111	0.110	0.007	8.494×10^{-12}
	2	10.78	468	0.152	0.151	0.010	8.867×10^{-12}
	3	3.07	364	0.0506	0.0505	0.002	8.336×10^{-12}
	3	14.96	364	0.198	0.196	0.009	1.020×10^{-11}
	4	5.26	416	0.0824	0.0821	0.003	8.994×10^{-12}

12. Additional Results for the Dual Mode Model

Figure S17 - S24 show additional examples of the agreement between experimental downstream pressure rise and simulations using a dual permeation modes for N_2 and CO_2, respectively. Tables S3 - S4 show the values of input variables for the dual mode model and its 3 scenarios.

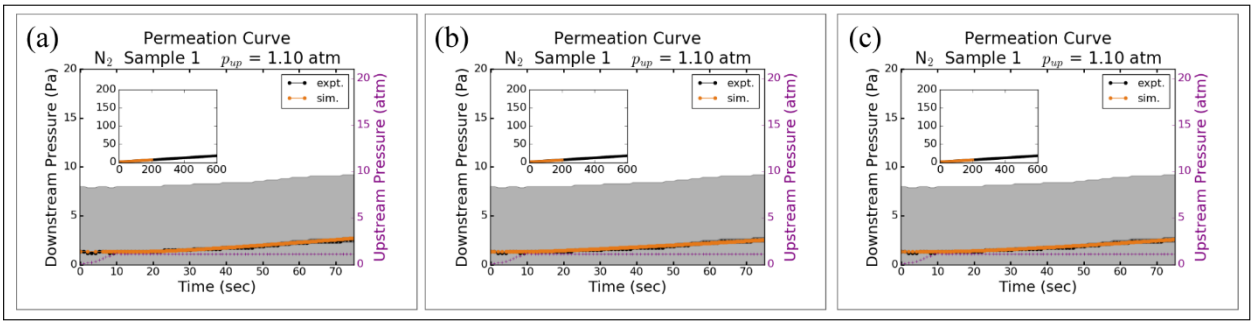

Figure S17. The downstream pressure increase over time as N_2 permeates through PPO using the dual mode model with (a) Scenario i, (b) Scenario ii, and (c) Scenario iii. The sample number and upstream pressure are given in the title. The inset shows the full experimental timescale, and the main figure zooms in on the pre-steady state region. The upstream pressure is included on the right y-axis. The shaded regions represent instrument error of 10%.

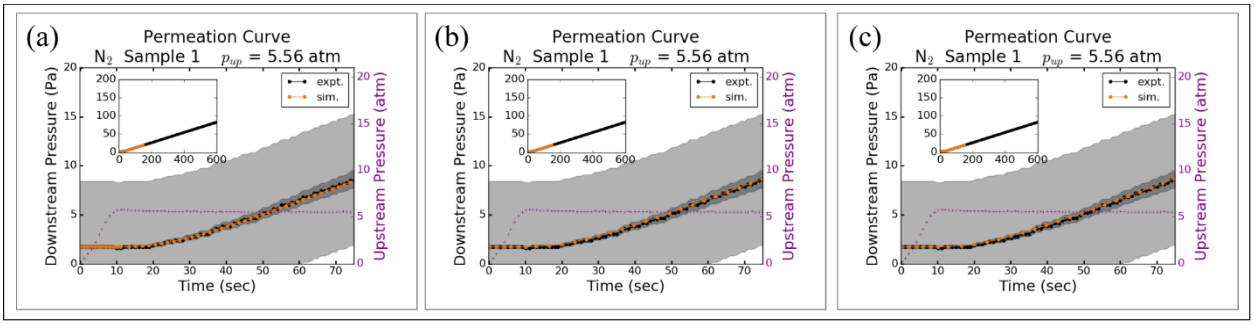

Figure S18. The downstream pressure increase over time as N_2 permeates through PPO using the dual mode model with (a) Scenario i, (b) Scenario ii, and (c) Scenario iii. The sample number and upstream pressure are given in the title. The inset shows the full experimental timescale, and the main figure zooms in on the pre-steady state region. The upstream pressure is included on the right y-axis. The shaded regions represent instrument error of 10%.

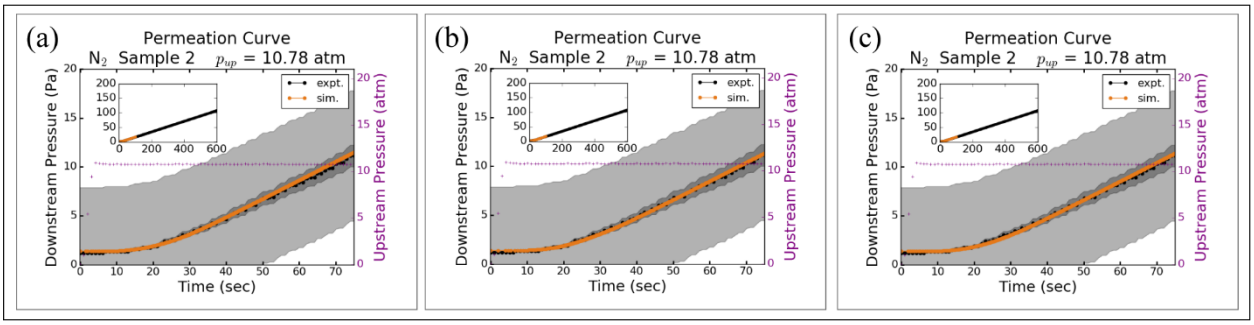

Figure S19. The downstream pressure increase over time as N_2 permeates through PPO using the dual mode model with (a) Scenario i, (b) Scenario ii, and (c) Scenario iii. The sample number and upstream pressure are given in the title. The inset shows the full experimental timescale, and the main figure zooms in on the pre-steady state region. The upstream pressure is included on the right y-axis. The shaded regions represent instrument error of 10%.

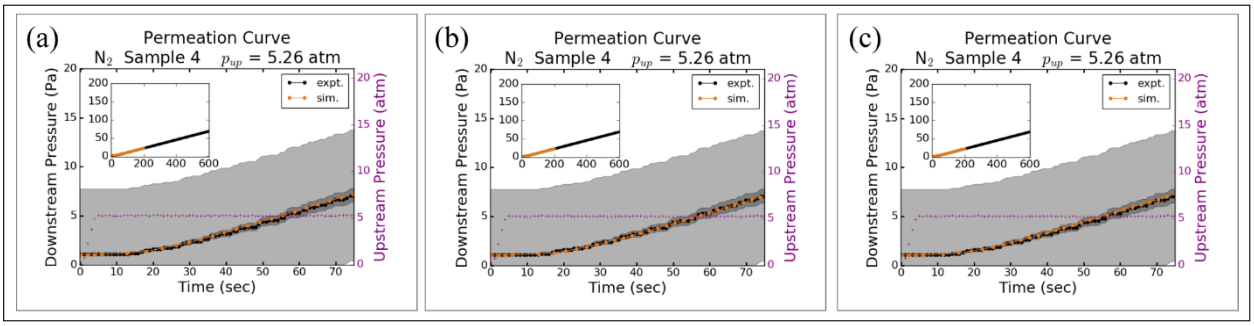

Figure S20. The downstream pressure increase over time as N_2 permeates through PPO using the dual mode model with (a) Scenario i, (b) Scenario ii, and (c) Scenario iii. The sample number and upstream pressure are given in the title. The inset shows the full experimental timescale, and the main figure zooms in on the pre-steady state region. The upstream pressure is included on the right y-axis. The shaded regions represent instrument error of 10%.

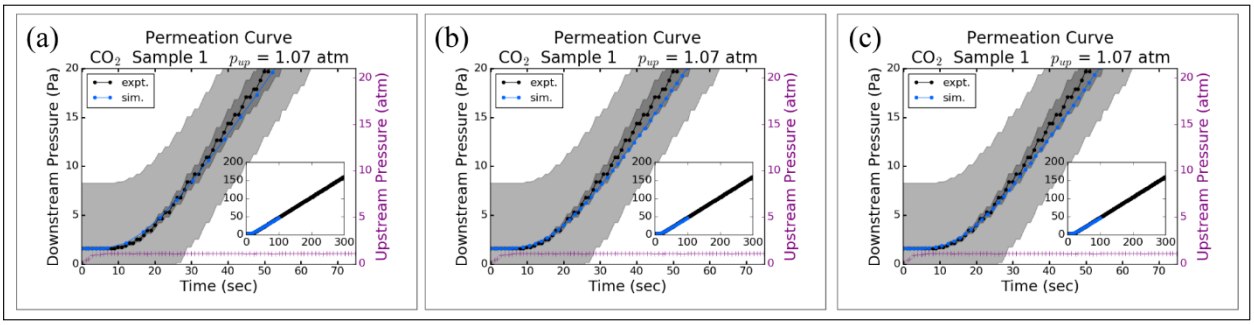

Figure S21. The downstream pressure increase over time as CO_2 permeates through PPO using the dual mode model with (a) Scenario i, (b) Scenario ii, and (c) Scenario iii. The sample number and upstream pressure are given in the title. The inset shows the full experimental timescale, and the main figure zooms in on the pre-steady state region. The upstream pressure is included on the right y-axis. The shaded regions represent instrument error of 10%.

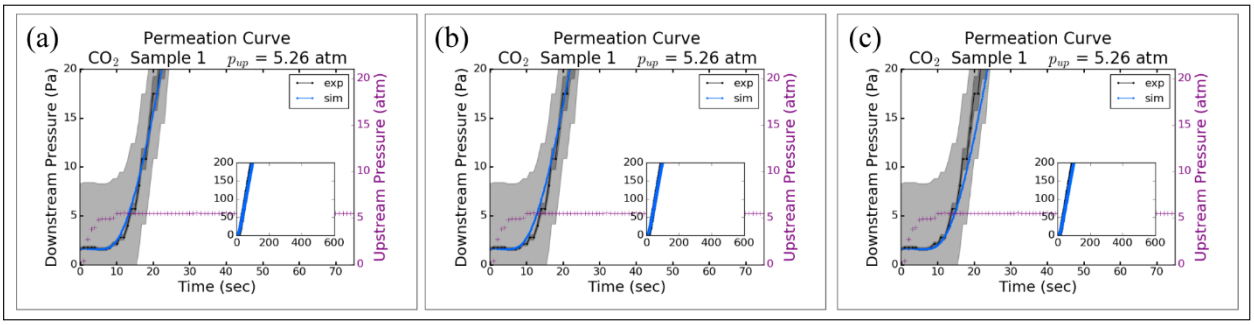

Figure S22. The downstream pressure increase over time as CO_2 permeates through PPO using the dual mode model with (a) Scenario i, (b) Scenario ii, and (c) Scenario iii. The sample number and upstream pressure are given in the title. The inset shows the full experimental timescale, and the main figure zooms in on the pre-steady state region. The upstream pressure is included on the right y-axis. The shaded regions represent instrument error of 10%.

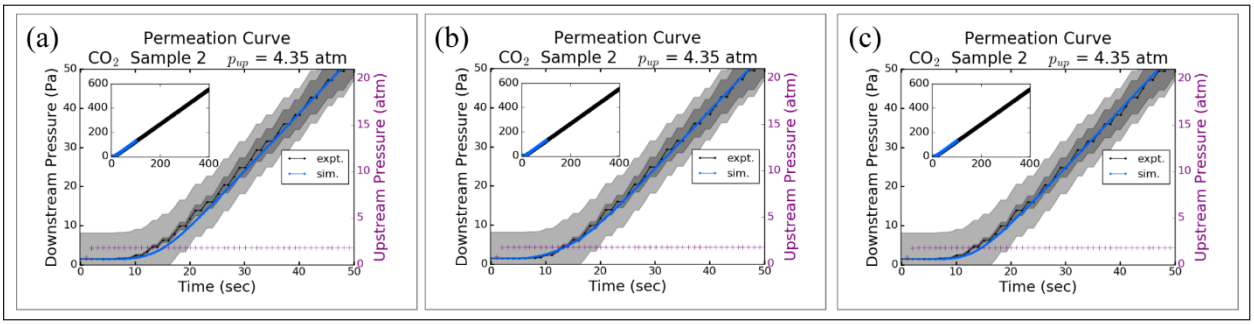

Figure S23. The downstream pressure increase over time as CO_2 permeates through PPO using the dual mode model with (a) Scenario i, (b) Scenario ii, and (c) Scenario iii. The sample number and upstream pressure are given in the title. The inset shows the full experimental timescale, and the main figure zooms in on the pre-steady state region. The upstream pressure is included on the right y-axis. The shaded regions represent instrument error of 10%.

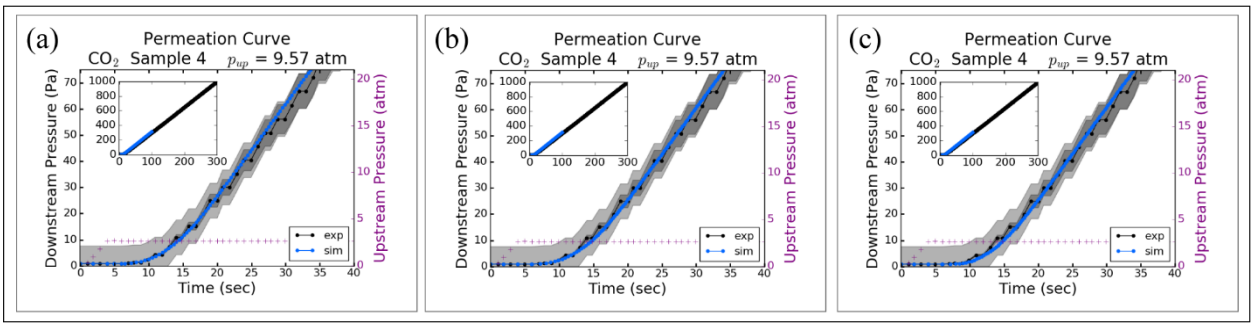

Figure S24. The downstream pressure increase over time as CO_2 permeates through PPO using the dual mode model with (a) Scenario i, (b) Scenario ii, and (c) Scenario iii. The sample number and upstream pressure are given in the title. The inset shows the full experimental timescale, and the main figure zooms in on the pre-steady state region. The upstream pressure is included on the right y-axis. The shaded regions represent instrument error of 10%.

Table S3. List of input variables for the dual mode simulations.

Gas	Sample	p_{up}	$[gas(g)]_{init}$	potential $[gas(p)]_{max}$ in Ψ_v^D	potential $[gas(p)]_{max}$ in Ψ_v^L	$[gas(p)]_{max}$ in Ψ_p^D	$[gas(p)]_{max}$ in Ψ_p^L
		atm	nmol/L	mol/L	mol/L	mol/L	mol/L
CO_2	1	1.07	624	0.0452	0.258	0.0446	0.255
	1	5.26	624	0.230	0.718	0.220	0.688
	2	4.35	572	0.189	0.656	0.182	0.631
	3	17.32	416	0.786	1.07	0.725	0.984
	4	9.57	364	0.425	0.906	0.400	0.854
N_2	1	1.10	520	0.00580	0.0131	0.00580	0.131
	1	5.56	676	0.0295	0.0570	0.0294	0.0568
	2	10.78	468	0.0573	0.0948	0.0569	0.0942
	4	5.26	416	0.0279	0.0545	0.0278	0.0543
	4	18.18	364	0.0971	0.133	0.0960	0.132

Table S4. Activation rate coefficient, k_{rise}, for each of the dual mode methods.

Gas	Sample	p_{up}	Scenario (i)	Scenario (ii)	Scenario (iii)	
		atm	$k^D{}_{rise}$	$k^D{}_{rise} = k^L{}_{rise}$	$k^D{}_{rise}$	$k^L{}_{rise}$
			M s^{-1}	M s^{-1}	M s^{-1}	M s^{-1}
CO_2	1	1.07	0.30	0.70	0.06	0.10
	1	5.26	0.50	0.20	0.06	0.10
	2	4.35	0.012	0.03	0.012	0.10
	3	17.32	0.06	0.08	0.06	0.10
	4	9.57	0.03	0.045	0.025	0.10
N_2	1	1.10	0.001	0.01	0.007	0.03
	1	5.56	0.003	0.01	0.007	0.03
	2	10.78	0.002	0.003	0.002	0.10
	4	5.26	0.001	0.0015	0.001	0.10
	4	18.18	0.003	0.004	0.003	0.10

13. Kinetic Diameter

The size of a molecule can be described in several ways. One measure is the critical volume, which describes the space filled by a molecule's electron cloud. Often, this volume is converted to a molecular diameter by assuming a spherical molecular shape, e.g., the Chung diameter.[16] Another measure of molecular size is the collisional diameter that is commonly reported in physical chemistry textbooks, e.g. Engel and Reid[11] and is derived from measurements of viscosity.[17] The collisional diameter is also commonly referred to as the Lennard-Jones (LJ) diameter since it is typically calculated using the LJ 12-6 interaction potential energy function

(PEF), again assuming a spherical molecular shape.[17] Though the assumption of spherical molecules is questionable in some cases (e.g., long chain alkanes), these diameters give an average measure of the space filled by a molecule - a fundamental molecular property. Values for critical volume and collisional diameter for a number of gases are reported in Table S5.

Table S5. Molecular Sizes from Ref. [16].

Gas	V_{crit}	d_{Chung}	σ_{LJ}
	cm^3/mol	Å	Å
He	57.5	3.123	2.551
H_2	64.9	3.251	2.827
O_2	73.5	3.389	3.467
N_2	89.3	3.616	3.798
CO	90.1	3.627	3.69
CO_2	91.9	3.651	3.941
H_2O	55.9	3.093	2.641
C_2H_4	131.1	4.11	4.163

For studies of transport through solid materials, the concept of a kinetic diameter is often used. Though the kinetic diameter is convenient for placing CO_2 within the trend of diffusion coefficient versus size for other light gases, it is problematic from a physical chemistry perspective since it is unclear what fundamental property the "kinetic diameter" is describing. Furthermore, we find that the commonly cited source for kinetic diameter, Breck's book *Zeolite Molecular Seives*,[18] is inconsistent in its calculation of kinetic diameter.

It is true that describing molecular size in terms of a single diameter can be misleading for oblong molecules. However, any correction for molecular shape should be applied consistently across all molecules, which does not appear to be the case for the kinetic diameters reported by Breck (reproduced in Table S6). His proposed correction equates to dividing the Pauling width by $2^{1/6}$, essentially assuming a LJ 12-6 PEF applied only to the smaller dimension. This leaves the question of which molecules should be subject to a shape correction. Breck's proposal seems to be that a molecule sorbed into a zeolite at equilibrium with pores smaller than the collisional diameter should receive a shape correction. In addition, the disparate physical and chemical natures of zeolites and polymers make it questionable to directly apply an observation of one to the other.

Another potential method is to define a cut-off in the length-to-width ratio (reported in Table S6), above which only the width should be used. For N_2 and CO_2, the length-to-width ratios are 1.37 and 1.38, respectively, which are very similar values and so it is still not clear why a shape correction should be applied to one and not the other. Additionally, Breck applies his shape correction to some molecules with a smaller length-to-width ratio (more spherical, e.g. SO_2) than N_2 but does not apply it to some molecules with a larger length-to-width ratio (more oblong, e.g. C_2H_2) than CO_2. When the shape correction proposed by Breck is applied consistently, N_2 is still the smaller molecule. Therefore, these should not be considered a fundamental measurement of the space occupied by a molecule in the way that critical volume and collisional diameters are.

Based on our assessment, it is likely that molecular interactions (e.g., polarizability) play a role in the kinetic diameters reported based on zeolite passage. In this case, the kinetic diameter of CO_2 falling within the trend of *P* and *D* versus size for other light gases could be fortuitous or may indicate the importance of polarizability in CO_2's interactions with both types of materials.

Table S6. Reanalysis of kinetic diameter calculations. The data on Pauling length, l_P, Pauling width, w_P, and kinetic diameter, d_k, are taken from Ref. [18]. The data on d_k are sorted based on the manner in which they were calculated by Breck, where σ_{LJ} is the diameter calculated using the Lennard-Jones potential, σ_{St} is the diameter calculated using the Stockmeyer potential, and *z* is the diameter estimated based on which zeolite sieves the molecule can pass through. The ratio of l_P/w_P and the size based on the smaller molecular dimension ($w_P/2^{1/6}$) are new calculations.

Gas	l_P	w_P	$\frac{l_P}{w_P}$	d_k			$\frac{w_P}{2^{1/6}}$
				σ_{LJ} *	σ_{St}	z	
	Å	Å		Å	Å	Å	Å
He	3	3	1	2.6			2.67
H_2	3.1	2.4	1.29	2.89			2.14
O_2	3.9	2.8	1.39 †	3.46			2.49
N_2	4.1	3	1.37	3.64			2.67
NO	4.05	3	1.35	3.17			2.67
N_2O	4.2	3.7	1.14 **			3.3	3.30
CO	4.2	3.7	1.14 **	3.76			3.30
CO_2	5.1	3.7	1.38			3.3	3.30
Cl_2	5.6	3.6	1.56			3.2	3.21
H_2O	3.9	3.15	1.24		2.65		2.81
NH_3	4.1	3.8	1.08		2.6		3.39
SO_2	5.28	4	1.32 ‡			3.6	3.56
C_2H_2	5.7	3.7	1.54 †	3.3			3.30
C_2H_4	5	4.4	1.14 ‡			3.9	3.92
C_3H_8	6.5	4.9	1.33 ‡			4.3	4.37

* $\sigma_{LJ} = r_{min} / 2^{1/6}$

** same ratio but shape correction applied to only one

† more oblong than CO_2 but shape correction not used

‡ less oblong than N_2 but shape correction applied

References

1. Toi, K.; Morel, G.; Paul, D. R., Gas Sorption and Transport in Poly(phenylene Oxide) and Comparisons with Other Glassy Polymers. *Journal of Applied Polymer Science* **1982,** *27*, 2997-3005.
2. Wright, C. T.; Paul, D. R., Gas Sorption and Transport in UV-Irradiated Poly(2,6-dimethyl-1,4-phenylene oxide) Films. *Journal of Applied Polymer Science* **1998,** *67*, 875-883.
3. Chern, R. T.; Sheu, F. R.; Jia, L.; Stannett, V. T.; Hopfenberg, H. B., Transport of Gases in Unmodified and Aryl-Brominated 2,6-Dimethyl-1,4-Poly(Phenylene Oxide). *Journal of Membrane Science* **1987,** *35*, 103-115.
4. Alentiev, A.; Drioli, E.; Gokzhaev, M.; Golemme, G.; Ilinich, O.; Lapkin, A.; Volkov, V.; Yampolskii, Y., Gas Permeation Properties of Phenylene Oxide Polymers. *Journal of Membrane Science* **1998,** *138* (1), 99-107.
5. Maeda, Y.; Paul, D. R., Effect of Antiplasticization on Gas Sorption and Transport. II. Poly(phenylene Oxide). *Journal of Polymer Science: Part B: Polymer Physics* **1987,** *25*, 981-1003.
6. Bondar, V. I.; Kamiya, Y.; Yampol'skii, Y. P., On Pressure Dependence of the Parameters of the Dual-Mode Sorption Model. *Journal of Polymer Science, Part B: Polymer Physics* **1996,** *34* (2), 369-378.
7. Potoff, J. J.; Siepmann, J. I., Vapor–Liquid Equilibria of Mixtures Containing Alkanes, Carbon Dioxide, and Nitrogen. *AIChE Journal* **2001,** *47* (7), 1676–1682.
8. Barducci, A.; Bussi, G.; Parrinello, M., Well-Tempered Metadynamics: A Smoothly Converging and Tunable Free-Energy Method. *Physical Review Letters* **2008,** *100* (2), 020603.
9. Linstrom, P. J.; Mallard, W. G., *NIST Chemistry WebBook, NIST Standard Reference Database Number 69*. National Institute of Standards and Technology: Gaithersburg MD.
10. *NIOSH Pocket Guide to Chemical Hazards*. U.S. Dept. of Health and Human Services, Public Health Service, Centers for Disease Control and Prevention, National Institute for Occupational Safety and Health: Washington, DC, 1994.
11. Engel, T.; Reid, P., *Thermodynamics, Statistical Thermodynamics, & Kinetics*. 2nd ed.; Prentice Hall: 2010.
12. Zhao, Y. H.; Abraham, M. H.; Zissimos, A. M., Fast Calculation of van der Waals Volume as a Sum of Atomic and Bond Contributions and Its Application to Drug Compounds. *Journal of Organic Chemistry* **2003,** *68*, 7368-7373.
13. Gotthardt, P.; Grüger, A.; Brion, H. G.; Plaetschke, R.; Kirchheim, R., Volume Change of Glassy Polymers by Sorption of Small Molecules and its Relation to the Intermolecular Space. *Macromolecules* **1997,** *30* (25), 8058-8065.
14. Visser, T.; Wessling, M., When do Sorption-Induced Relaxations in Glassy Polymers Set In? *Macromolecules* **2007,** *40* (14), 4992-5000.
15. Lin, H.; Freeman, B. D., Gas Solubility, Diffusivity and Permeability in Poly(Ethylene Oxide). *Journal of Membrane Science* **2004,** *239* (1), 105–117.
16. Yampolskii, Y. P.; Pinnau, I.; Freeman, B. D., *Materials Science of Membranes for Gas and Vapor Separation*. John Wiley & Sons Ltd: West Sussex, England, 2006; p 445-445.
17. Poling, B. E.; Prausnitz, J. M.; O'Connell, J. P., *The properties of gases and liquids*. 5th ed.; McGraw-Hill, Inc.: New York, 2001.
18. Breck, D. W., *Zeolite molecular sieves: structure, chemistry, and use*. R.E. Krieger: 1984.